ADVANCED ELECTRONIC MATERIALS
www.advelectronicmat.de

Routes for Efficiency Enhancement in Fluorescent TADF Exciplex Host OLEDs Gained from an Electro-Optical Device Model

Markus Regnat, Kurt P. Pernstich, Kwon-Hyeon Kim, Jang-Joo Kim, Frank Nüesch, and Beat Ruhstaller*

Fluorescence-based organic light-emitting diodes (OLEDs) using thermally activated delayed fluorescence (TADF) have increasingly attracted attention in research and industry. One method to implement TADF is based on an emitter layer composed of an exciplex host and a fluorescent dopant. Even though the experimental realization of this concept has demonstrated promising external quantum efficiencies, the full potential of this approach has not yet been assessed. To this end, a comprehensive electro-optical device model accounting for the full exciton dynamics including triplet harvesting and exciton quenching is presented. The model parameters are fitted to multiple output characteristics of an OLED comprising a TADF exciplex host with a fluorescent emitter, showing an external quantum efficiency of >10%. With the model at hand, an emission zone analysis and a parameter study are performed, and possible routes for further efficiency enhancement are presented.

1. Introduction

The recent discovery of thermally activated delayed fluorescence (TADF) by the Adachi group[1–4] attracted a lot of attention in research and industry. It was found that an organic light-emitting diode (OLED) with a fluorescent emitter material having a very small energy difference between the triplet and singlet states facilitates reverse intersystem crossing of triplets to singlets at room temperature, resulting in an increased efficiency. This discovery opened the possibility to fabricate highly efficient fluorescence-based OLEDs with external quantum efficiencies (EQEs) similar to phosphorescence-based OLEDs, but with the advantages of a broader variety of emitter materials (no iridium and platinum complexes), higher color purity, and higher operational stability.[5]

Different TADF approaches are presently employed to increase the efficiency of fluorescent OLEDs including TADF emitter molecules, TADF assistant dopant molecules, TADF exciplex hosts, and different combination of them. With TADF emitters in a conventional host,[6] an exciplex host,[7] or in a TADF exciplex host,[8] EQEs of up to 37% were obtained without light outcoupling structures, which are similar to the values obtained with the best phosphorescent OLEDs.[9] By adding TADF assistant dopants to fluorescent emitters in conventional hosts[5,10,11] or in a TADF exciplex host,[12] EQEs of up to 24% were reported. The third class uses TADF exciplex hosts with conventional fluorescent emitters, and EQEs of >10%[10,13] are currently reached. The OLEDs investigated in this study are of this type.

While many different approaches to fabricate TADF OLEDs are pursued, modeling of TADF OLEDs has received only little attention.[8,14,15] In this study, we present, to the best of our knowledge, the first electro-optical device model that accounts for charge carriers, excitons, and photons, to describe the electro-optical characteristics of an OLED with a fluorescent dye in a TADF exciplex host.[13] The model reproduces the current–voltage–luminance (I–V–L) characteristics, the angle-dependent electroluminescence (EL) spectra, and the EL decay. From the angle-dependent measurements, the emission zone (EMZ) profile is determined.[16–19] The knowledge of the EMZ profile is, among others, important to set the exciton diffusion constant. Surprisingly, a split EMZ is found, where large exciton densities are present at both interfaces of the emitting layer. The model also reveals the strongly bias-dependent triplet harvesting contribution to the EQE. From a model parameter study, several routes are proposed for further optimization of the OLED stack and the increase of the EQE. The simulations identify

M. Regnat, Dr. K. P. Pernstich, Prof. B. Ruhstaller
Institute of Computational Physics
Zurich University of Applied Sciences ZHAW
8401 Winterthur, Switzerland
E-mail: markus.regnat@zhaw.ch
M. Regnat, Prof. F. Nüesch
Institut des Matériaux
Ecole Polytechnique Fédérale de Lausanne, EPFL
Station 12,1015 Lausanne, Switzerland
Dr. K.-H. Kim, Prof. J.-J. Kim
Department of Materials Science and Engineering
Seoul National University
Seoul 151-742, South Korea
Prof. B. Ruhstaller
FLUXIM AG
Technoparkstrasse 2, 8406 Winterthur, Switzerland
The ORCID identification number(s) for the author(s) of this article can be found under https://doi.org/10.1002/aelm.201900804.

DOI: 10.1002/aelm.201900804

that increasing the intersystem crossing rate or reducing the triplet–triplet annihilation rate results in the largest improvement of the EQE. In the best case scenario, efficiencies up to 42% are predicted.

2. Modeling and Model Parameters

To establish the electro-optical OLED device model, a preview version of the simulation software Setfos version 5.0 from Fluxim, Inc. with the drift-diffusion and emission module was used.[20] For further details on the charge carrier drift-diffusion and recombination, exciton migration, and radiative dipole emission model implemented in Setfos refer to ref. [21–23]. Initial input parameters for the electro-optical model, such as layer thicknesses, (birefringent) refractive indices, discrete highest and lowest molecular orbital (HOMO/LUMO) energy levels,[24–26] field-dependent electron and hole mobilities,[27–29] as well as excitonic parameters in the emission layer (EML)[13,25,30] were either directly measured or taken from literature. The model parameters were manually adjusted in a way that the simulation results agree with the measurements described below, that is, the I–V–L characteristics and the angle-dependent EL spectra. The optimized model parameters are given in **Figure 1**; Figure S1 and Table S1, Supporting Information.

Figure 1 shows the OLED layer stack with layer thicknesses and the frontier orbital energy levels of each layer. The OLEDs were fabricated as described in detail by Kim et al.,[13] and the details of the model are described by Perucco et al.[19] and Regnat et al.[31] The emissive layer comprises co-evaporated tris(4-carbazoyl-9-ylphenyl)amine (TCTA) and 4,6-bis(3,5-di(pyridin-4-yl)phenyl)-2-methylpyrimidine (B4PYMPM) (1:1 molar ratio), doped with 0.5 wt% 4-(dicyanomethylene)-2-*tert*-butyl-6-(1,1,7,7-tetramethyljulolidin-4-yl-vinyl)-4*H*-pyran (DCJTB). The EML was modeled with a hole mobility and HOMO energy level similar to TCTA and an electron mobility and LUMO energy level similar to B4PYMPM in order to reproduce the measured current–voltage characteristics. We like to note that the HOMO/LUMO levels of the co-evaporated exciplex host are often assumed to be identical to the respective energy levels of the pure constituent materials, but we did not find a parameter set with such identical energy levels that gave a good agreement to the measurements. That the energy levels can change upon co-evaporation has been reported before[32] and, thus, the reported HOMO/LUMO energy levels for the exciplex host appear feasible.

To determine the EMZ profile from combined measurements and simulations, optically detuned OLEDs had to be fabricated.[16–18] This was achieved by increasing the thickness of the doped electron transport layer (ETL) from 28 nm for the optically tuned OLED that maximizes EQE/light output to 128 nm for the detuned OLED. The doped ETL was modeled by introducing an electron donor doping concentration of 2.4×10^{25} m^{-3} and removing the field dependence of the electron mobility. This concentration was chosen in order to reproduce the measured current–voltage characteristics for optically tuned and detuned OLEDs.

To accurately simulate the luminance, current efficiency, EQE, and angle-dependent EL spectra, multiple excitonic processes had to be considered in the EML as illustrated in **Figure 2**: Singlet and triplet exciplex generation on the exciplex host is modeled via Langevin recombination of electrons and holes, where a singlet-to-triplet ratio of 1:3 is considered by the exciplex generation factors $g_s = 0.25$ and $g_t = 0.75$. Host triplets are converted to host singlets with a reverse intersystem crossing rate

$$k_{\mathrm{RISC}} = k_{\mathrm{ISC}} e^{\frac{-\Delta E_{S/T}}{k_B T}} \tag{1}$$

where k_{ISC} is the intersystem crossing rate from host singlets to triplets and $\Delta E_{S/T}$ is the energy difference between those states. As illustrated in Figure 2, host triplets can recombine only nonradiatively as reported by Kim et al.,[25] while host singlets can recombine radiatively and nonradiatively. The host singlets can also transfer their energy to the fluorescent DCJTB emitter via Förster resonance and Dexter energy transfer with a rate constant of $k_{\mathrm{FRET/DEX}} = 1$ ns^{-1}. In the model, this rate constant was estimated to reproduce the weak light emission originating from the host singlets that was observed in the measurements. The guest emitter is modeled as having a singlet state that can

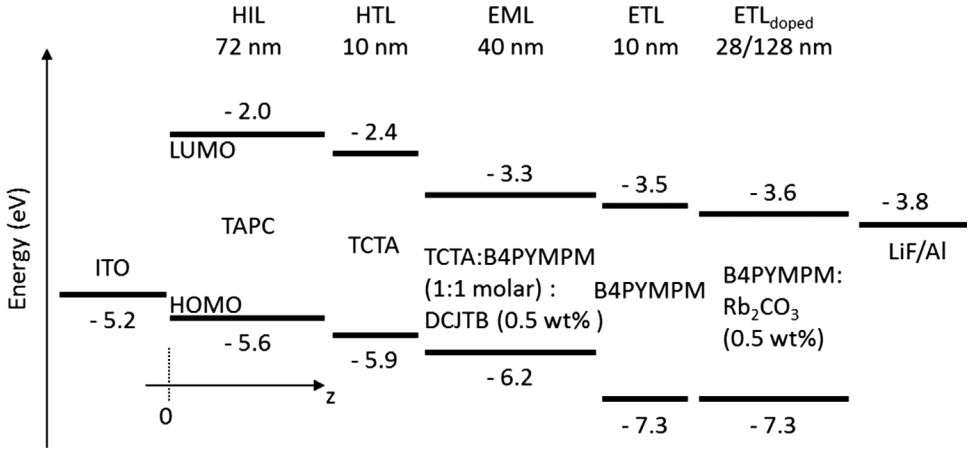

Figure 1. Layer stack of the TADF exciplex host OLED with the layer thicknesses and the HOMO/LUMO energy levels used in the simulations. In the optically detuned OLED, the thickness of the doped ETL was increased from 28 to 128 nm.

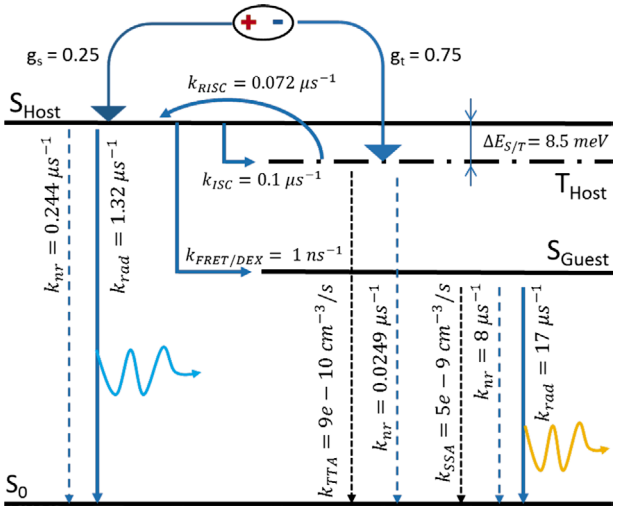

Figure 2. Illustration of the excitonic processes in the emission layer of the TADF exciplex host OLED with fluorescent emitter. See text for details.

recombine radiatively and nonradiatively. The dipole orientation of the emitter molecules is set to be 86% horizontal,[13] and the photoluminescence spectra of the host and guest emitters are taken from the study by Li et al.[12] and are reproduced in Figure S2, Supporting Information. Annihilation of both host triplet exciplexes and guest singlet excitons had to be included in the model with the rate constants of $k_{TTA} = 9 \times 10^{-10}$ cm^3 s^{-1} and $k_{SSA} = 5 \times 10^{-9}$ cm^3 s^{-1} to accurately reproduce the measurement data. The host k_{TTA} is as high as in single crystalline tetracene,[33] which is surprising. Initial attempts to additionally include triplet polaron quenching on the host, which could lead to a lower k_{TTA}, did not yield a good agreement with the measured current efficiency. This suggests that the k_{TTA} on the exciplex host might indeed be rather high. The three continuity rate equations for the exciton and the exciplexes are given in the Supporting Information.

To model the spatial extent of the EMZ as determined from the optically detuned OLED measurements, exciton diffusion was enabled only for the guest singlet excitons with a diffusion constant of 900 nm^2 µs^{-1}. Exciton diffusion is often described to occur via Förster resonance or Dexter energy transfer, in which a spectral overlap between the emission and absorption spectra is required. From the absorption and emission spectra presented in the study by Kim et al.[13] (reproduced in Figure S2, Supporting Information), we conclude that the spectral overlap integral between two TCTA/B4PYMPM host complexes essentially vanishes, while it is non-zero for the DCJTB guest molecules. From this, we derived the assumption of exciton diffusion occurring only between guest molecules, even though the distance between guest molecules is much larger than those between host molecules. If only the host exciplexes would diffuse, the exciplex density profile changes significantly as shown in Figure S4, Supporting Information, but with slightly modified model parameters, especially an increased triplet–triplet annihilation rate, the same agreement between measurement and simulation can be obtained.

3. Electro-Optical Characterization

Figure 3a shows the excellent agreement between the simulated and the measured current density–voltage–luminance characteristics for the optically tuned and detuned OLEDs. The J–V characteristics for the tuned and detuned OLEDs is essentially identical due to the doped ETL, and only the light emission differs significantly as expected from the inset to Figure 3a. The electro-optical model parameter set was optimized to reproduce the measured data of the tuned OLED, and only the ETL_{doped} thickness was changed to simulate the detuned OLED. The minor deviations between simulated and measured J–V–L characteristics are attributed to variations during device manufacturing, while the minor deviations in current density at very low bias (<1.5 V) are caused by solver settings.

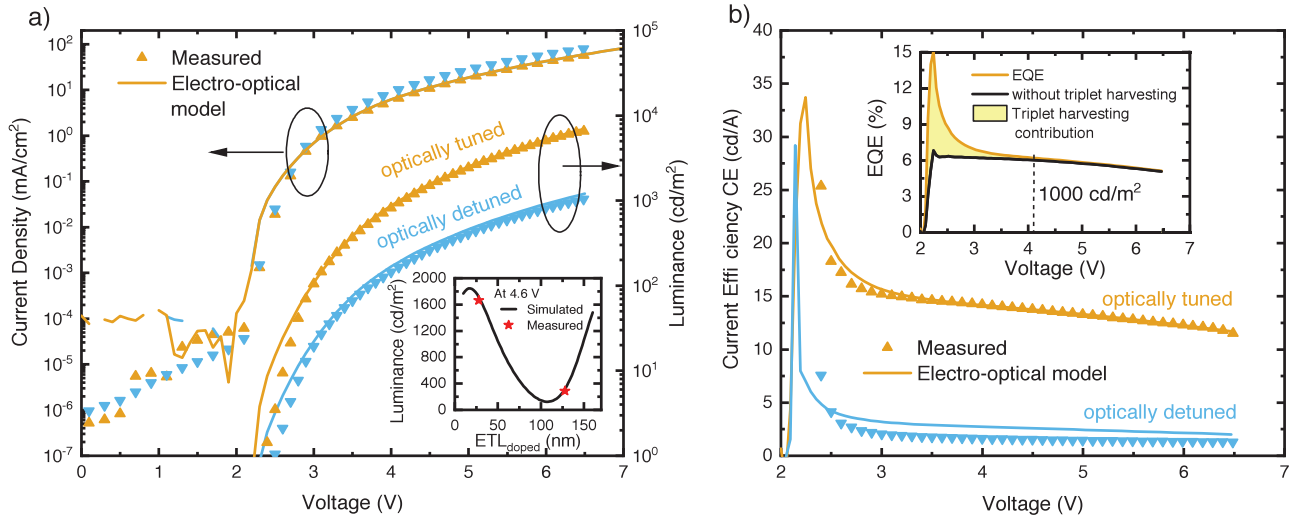

Figure 3. Measured and simulated current density–voltage–luminance curves a) and current efficiency b) for optically tuned (ETL_{doped} = 28 nm) and detuned (ETL_{doped} = 128 nm) OLEDs. The inset to a) shows the dependence of the luminance on the ETL_{doped} layer thickness and the inset to b) shows the simulated EQE for the optically tuned OLED together with the contribution of triplet harvesting to the EQE.

Figure 3b shows the measured and simulated current efficiencies that were calculated from the luminance and current density data in Figure 3a. The current efficiency is highest right after turn-on of the OLED at ≈2.2 V and decreases rapidly up to ≈2.9 V and less pronounced at higher biases. To model these two regimes, triplet–triplet annihilation on the host and singlet–singlet annihilation on the guest had to be considered as discussed in detail in Section 5. The inset to Figure 3b shows the bias dependence of the EQE for the optically tuned OLED (orange line) together with the contribution of triplet harvesting (shaded area). At low biases, very high efficiencies of up to 15% are obtained due to triplet harvesting. These EQEs are much higher than the theoretical limits for fluorescence-based OLEDs using only singlet excitons for light emission as shown with the black line in the inset to Figure 3b, where the triplet harvesting process was switched off by deactivating reverse intersystem crossing in the model. Surprisingly, the simulations suggest that the triplet harvesting is only significant at low biases where the luminance is well below ≈100 cd m^{-2} (cf. Figure 8).

4. EMZ Characterization

The knowledge of the EMZ profile and its bias dependence can have a significant influence on the OLED efficiency.[31] Therefore, the EMZ profile was determined in the optically detuned OLED from angle-dependent, s-polarized EL spectra measurements using a purely optical model as described earlier.[16] The optical model nicely reproduces the measured angle-dependent EL spectra shown in **Figure 4**a, and yields the EMZ profile shown in **Figure 5**. Determining the EMZ at a larger current density revealed essentially the same EMZ as for the lower current density (cf. Figure S3, Supporting Information). The bias-independent EMZ implies that the field dependence of the electron and the hole mobility is similar, otherwise a significant shift of the EMZ is expected as reported on in a previous study on a phosphorescent OLED.[17]

The angle-dependent EL spectra and the EMZ profile can also be obtained from the electro-optical model. Figure 4 shows the excellent agreement of the simulated EL spectra with the measurements for the detuned and tuned OLEDs, and the insets to Figure 4 show the measured and simulated angle-dependent radiance illustrating the strong influence of the optical detuning on the radiation pattern. The agreement between the EMZ profile in the detuned OLED obtained from the purely optical model and the one obtained from the electro-optical model (cf. Figure 5) highlights the validity of the electro-optical model. The width of the measured EMZ was used to estimate the exciton diffusion constant; thus, the measurements in the detuned OLED were essential to set this important model parameter. The inset to Figure 5 shows the Purcell factor, which is significantly larger at the HTL/EML interface in the tuned OLED, which causes the increased radiative dipole density at the HTL/EML interface in the tuned OLED compared to the detuned OLED.

Interestingly, a split EMZ was obtained, where large exciton densities are present at both interfaces of the EML.[17,34,35] This is explained by the good charge injection into the EML from the transport layers and the good charge blocking at the opposite EML interface, which leads to an accumulation of electrons and holes at the respective interfaces and an increased exciton density via Langevin recombination. The presence of a split EMZ is substantiated by the occurrence of an EL turn-off peak as discussed next. We note that in very similar systems,[26,36] no such turn-off peak and a homogeneous EMZ were observed, thus the EMZ profile appears to depend sensitively on the OLED stack.

In a recent study,[17] we have shown that the occurrence of a peak in the EL decay after the OLED is turned off[37] is a hallmark of a split EMZ. Therefore, **Figure 6** shows the measured and simulated EL decay of the tuned OLED. Unfortunately, the EL decay was measured in an aged device with significantly reduced current at a given voltage as shown in the inset to Figure 6. To model the degradation, we included hole traps in the HTL and reduced the (non-)radiative rates of the fluorescent

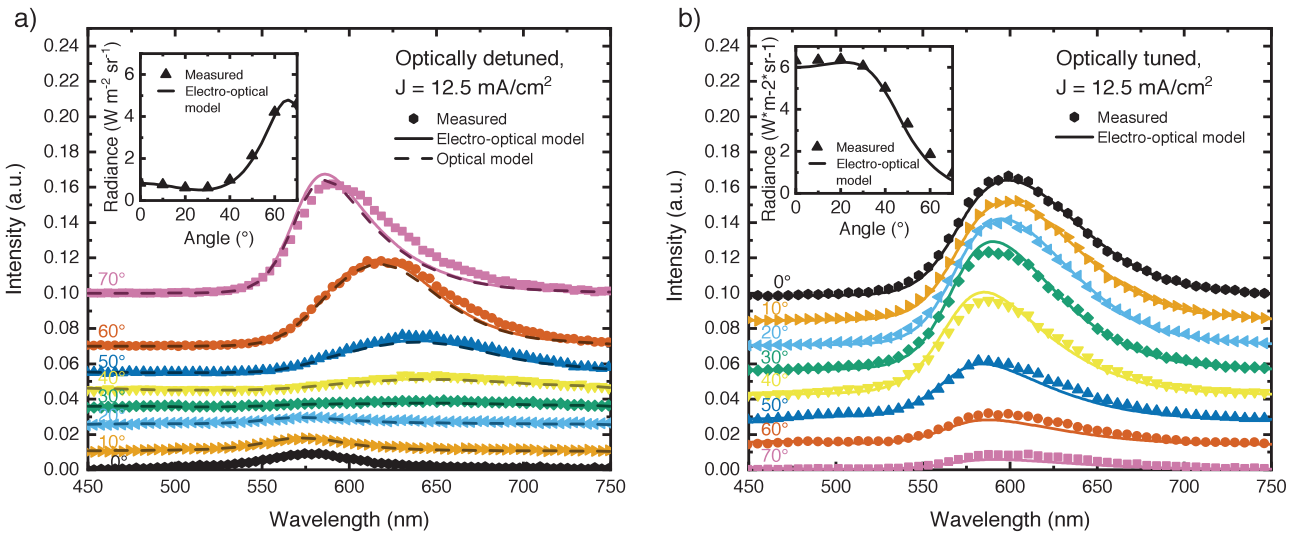

Figure 4. Angle-dependent s-polarized EL spectra at 12.5 mA cm^{-2} for optically detuned a) and tuned b) OLEDs obtained from measurements (symbols), the optical model (dashed lines), and the electro-optical model (solid lines). The insets show the measured and simulated integrated intensity (radiance) over the emission angle.

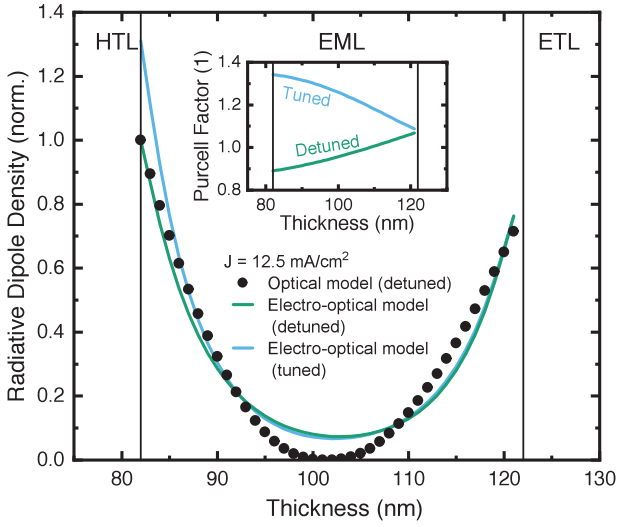

Figure 5. Radiative dipole density (emission zone) in the detuned and the tuned OLED obtained from the optical model (symbols) and the electro-optical model (lines).

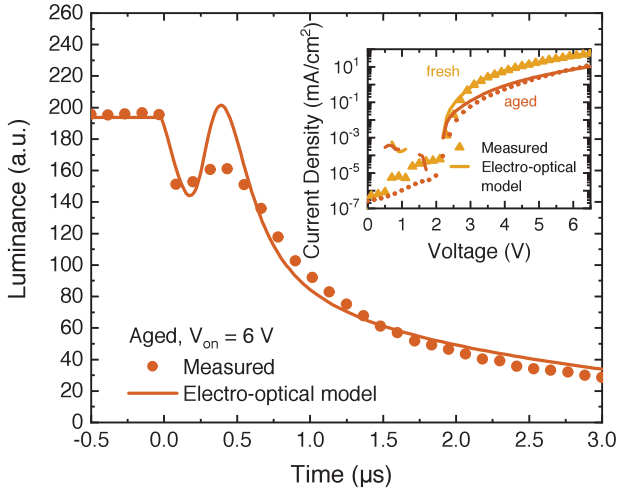

Figure 6. Measured and simulated EL decay for an on-voltage of 6 V of the aged, optically tuned OLED. The peak at 0.4 μs after turn-off signifies the presence of a split emission zone. The inset shows the measured and simulated current density–voltage curves for the fresh and the degraded OLED.

emitter. The simulation of the EL decay agrees only qualitatively with the measurements because the EL decay was not included as a fit target during optimization of the model parameters. Nevertheless, these measurements strongly support the findings of a split EMZ in our TADF OLEDs and suggest that split EMZs occur in phosphorescent[31] and TADF OLEDs alike.

5. Efficiency Enhancement Routes

Assuming an exponentially decaying EMZ with a maximum at the HTL/EML interface (profile I in **Figure 7**a), an optimum thickness of 28 nm is obtained (green line in Figure 7b). The measurements on the detuned OLED, as well as the electro-optical model, revealed a split EMZ (profile IV in Figure 7a), which results in a reduction of 6% in EQE for this layer thickness. Using the correct profile, an optimal thickness of 35 nm is obtained, which increases the EQE by 1.2% with respect to the fabricated OLED as indicated in Figure 7b.

If the EMZ would have a maximum at the EML/ETL interface (profile VI in Figure 7a), the thickness would need to be increased by 17 nm to achieve the highest EQE. The other profiles shown in Figure 7a result in a similar EQE variation, where the maximum EQE can be obtained from EMZ with a maximum emission in the center of the EML (profile II) or at the HTL/EML interface (profile I). Tuning the charge carrier mobilities in the host, respectively their field dependence, together with the energy barriers at the EML interfaces can, thus, provide a means to optimize the EQE. These simulations emphasize the importance of knowing the exact EMZ profile when optimizing the layer stack. We like to point out that the EMZ profile not only influences the light outcoupling as simulated in Figure 7, but also exciton quenching. The influence of exciton quenching was not included in the simulations leading to Figure 7b, but will be discussed next.

In **Figure 8**, the influence of various model parameters on the EQE is shown, where the orange line in all panels indicates the baseline simulations discussed above reproducing the experimental OLED data. Both nonradiative pathways on the host are sufficiently slow so that their influence on improving the EQE is negligible and are, thus, not shown. When varying the degree of horizontal orientation of the emitting dipoles (EDO) as shown in Figure 8a, the EQE is increased by essentially the same amount at all luminance levels. At 1000 cd m^{-2}, this increase amounts to 22% that motivates further optimization of the dipole orientation.

A larger increase in EQE can be obtained when the photoluminescence quantum yield (PLQY) of the DCJTB emitter is increased. The change of PLQY was modeled by either decreasing the nonradiative decay rate k_{nr} in the emitter (solid lines in Figure 8b) or by increasing the radiative decay rate k_{rad} (broken lines in Figure 8b). In both cases, the EQE increases essentially by the same value at all luminance values up to ≈1000 cd m^{-2} with increasing PLQY. To increase the EQE at even higher luminance levels, the radiative decay rate needs to be larger. A twofold increase of k_{rad} is already sufficient to increase the EQE at high luminance levels (dashed line in Figure 8b), and a further increase to very high values (dotted line in Figure 8b) does not bring a significant benefit.

In Figure 8c, the influence of the energy barrier $\Delta E_{S/T}$ is shown. In the chosen exciplex host, this value of 8.5 meV is already very low, and a further reduction to 3.5 meV only marginally increases the EQE by 0.6% at 1000 cd m^{-2}. At room temperature, energy barriers of 20 meV are already very effective in harvesting triplets at low luminance levels.

Another parameter describing the triplet harvesting process is the intersystem-crossing rate k_{ISC}, which influences the reverse intersystem-crossing rate k_{RISC} according to Equation (1). Figure 8d shows a pronounced drop in EQE at low luminance levels in the fabricated OLED. A tenfold increase in k_{ISC} strongly influences the EQE at lower luminance values, and at 1000 cd m^{-2}, this increase amounts to 24%. Increasing the

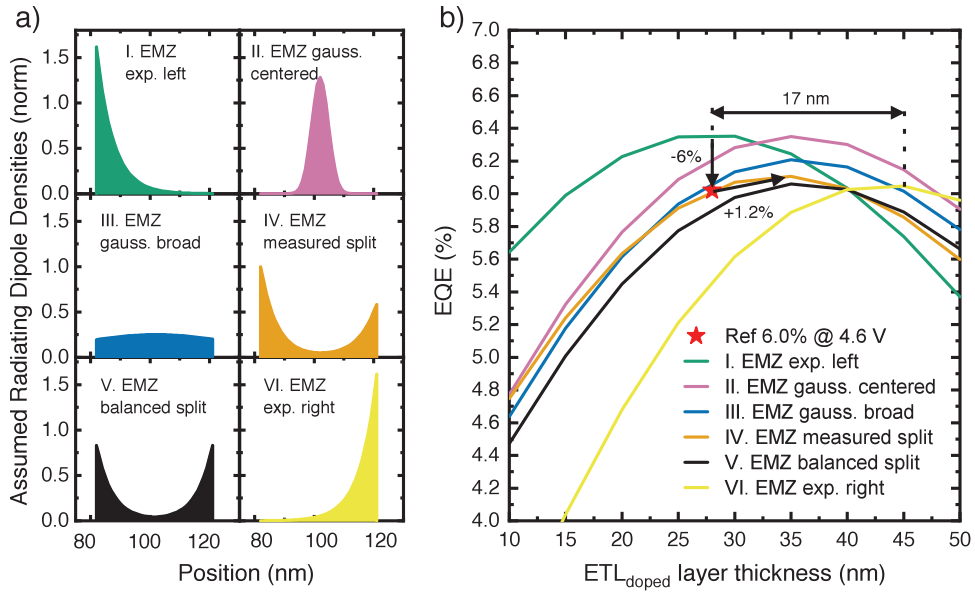

Figure 7. Influence of EMZ profiles a) on the EQE b) as obtained from optical simulations. Depending on the EMZ profile, the optimum thickness can vary up to 17 nm, resulting in a 6% change of the EQE. The marker indicates the tuned OLED described in this study.

intersystem crossing rate further extends the high EQE range to larger luminance values. Increasing k_{ISC} beyond 100 μs^{-1} has no significant effect on the EQE. The rational for this increase is that the host singlet density is rather low due to the very efficient transition of host singlets to guest singlets ($k_{FRET/DEX}$ in Figure 2). Thus, the increased intersystem crossing has a minor influence on the triplet density, and the increased triplet harvesting through reverse intersystem crossing dominates the effect on EQE.

Two additional influential model parameters are the triplet–triplet exciplex annihilation rate k_{TTA} on the host and the singlet–singlet exciton annihilation rate k_{SSA} on the guest as illustrated in Figure 8e. A tenfold decrease in k_{TTA} increases the EQE by 10% at 1000 cd m^{-2}. Lowering the value of k_{TTA} reveals a plateau in EQE with a drop-off at high luminance values, even if triplet–triplet annihilation on the host is completely turned-off. Reducing k_{SSA} on the other hand influences the EQE at high luminance values (dashed lines in Figure 8e). If

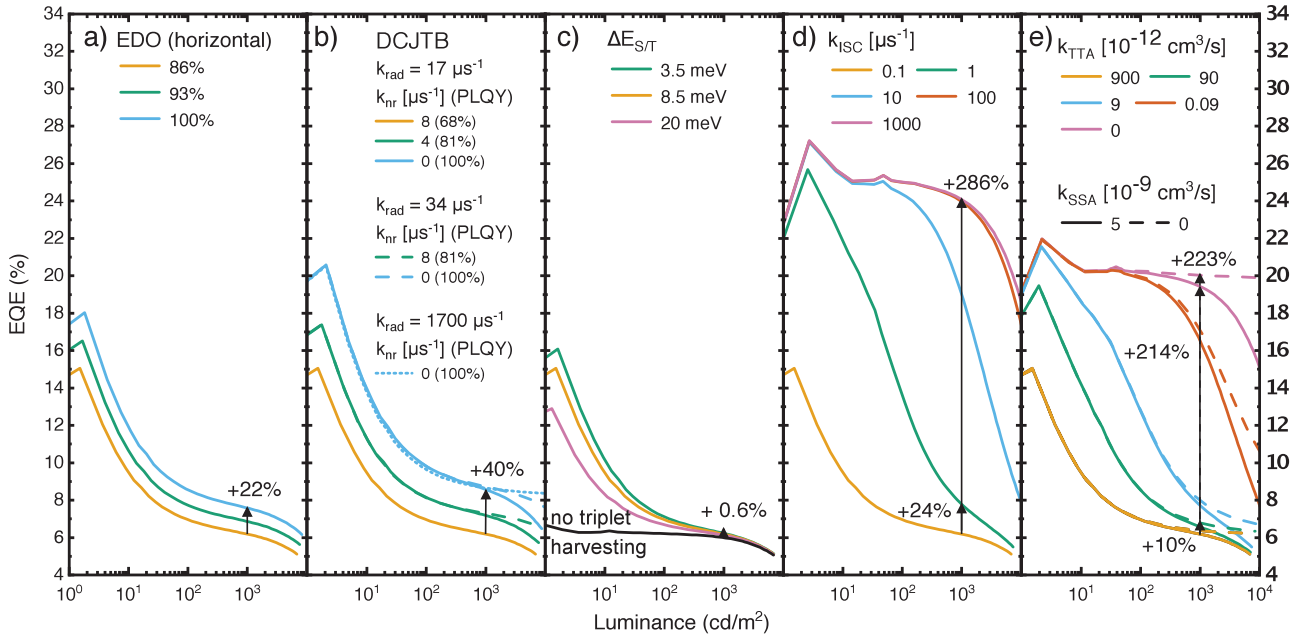

Figure 8. Influence of selected model parameters on EQE. The largest improvements can be realized by increasing the intersystem crossing rate k_{ISC} and by reducing the triplet–triplet annihilation rate.

both mechanisms are turned-off, no EQE roll-off at high luminance is observed. A low triplet density on the host is, thus, critical for device efficiency. To realize a high efficiency, a fast intersystem crossing rate and a reduced host TTA are essential. Besides reducing the k_{TTA} itself, tailoring the charge carrier mobilities to obtain a broad EMZ might also provide a pathway to enhanced efficiencies. In a best case scenario, where all efficiency enhancements predicted in Figure 8 can be realized, the model predicts an EQE of ≈42% even at high brightness of 1000 cd m^{-2} (cf. Figure S5, Supporting Information).

In conclusion, a comprehensive electro-optical model of an OLED with a TADF exciplex host and a fluorescent emitter was presented. The model considers charge transport, accounts for the full exciton dynamics including the triplet harvesting effect and light outcoupling. The investigated state-of-the-art OLEDs show EQEs >10% at low bias. Measurements reveal a split EMZ with high radiating dipole densities at both interfaces of the EML, which is nicely reproduced by the model. With the knowledge of the EMZ profile, the layer stack can be more accurately optimized for maximum efficiency. A parameter study showcases the effects of various model parameters on the efficiency. The most influential parameters are the (reverse) intersystem crossing rates between the singlet and triplet states on the host, and the triplet–triplet annihilation rate on the host. This work shows that electro-optical device modeling is a powerful tool to elucidate the details of charge carrier and exciton dynamics in TADF OLEDs and to guide future materials and device development.

6. Experimental Section

The fabrication details of the investigated optically tuned and detuned OLEDs are described in detail by Kim et al.[13]

All electro-optical measurements were taken with the all-in-one measurement system Paios and the Characterization Suite 4.2 from Fluxim.[38] For measuring the transient EL decay, a gated photomultiplier (H11526 Series) from Hamamatsu was used. The angle-dependent EL spectra were measured with a home-built goniometer add-on to Paios.[17] The goniometer used a cylindrical lens to prevent light trapping due to total internal reflection in the glass substrate. The current efficiency was calculated from the steady-state luminance and the current density.

Supporting Information

Supporting Information is available from the Wiley Online Library or from the author.

Acknowledgements

The authors thank S. Jenatsch, B. Blülle, S. Züfle, A. Stous, and A. Gentsch from Fluxim AG and J. Dunst and C. Kirsch from ZHAW for fruitful discussions and valuable comments. Financial support from the Swiss National Science Foundation under grant no. 162230 as well as from Korean National Research Foundation (KNRF) is gratefully appreciated.

Conflict of Interest

The authors declare no conflict of interest.

Keywords

electro-optical simulations, exciton dynamics, split emission zones, triplet harvesting, triplet–triplet annihilation

Received: July 31, 2019
Revised: November 5, 2019
Published online:

[1] A. Endo, K. Sato, K. Yoshimura, T. Kai, A. Kawada, H. Miyazaki, C. Adachi, *Appl. Phys. Lett.* **2011**, *98*, 083302.
[2] H. Uoyama, K. Goushi, K. Shizu, H. Nomura, C. Adachi, *Nature* **2012**, *492*, 234.
[3] Q. Zhang, B. Li, S. Huang, H. Nomura, H. Tanaka, C. Adachi, *Nat. Photonics* **2014**, *8*, 326.
[4] S. Hirata, Y. Sakai, K. Masui, H. Tanaka, S. Y. Lee, H. Nomura, N. Nakamura, M. Yasumatsu, H. Nakanotani, Q. Zhang, K. Shizu, H. Miyazaki, C. Adachi, *Nat. Mater.* **2015**, *14*, 330.
[5] H. Nakanotani, T. Higuchi, T. Furukawa, K. Masui, K. Morimoto, M. Numata, H. Tanaka, Y. Sagara, T. Yasuda, C. Adachi, *Nat. Commun.* **2014**, *5*, 4016.
[6] T.-A. Lin, T. Chatterjee, W.-L. Tsai, W.-K. Lee, M.-J. Wu, M. Jiao, K.-C. Pan, C.-L. Yi, C.-L. Chung, K.-T. Wong, C.-C. Wu, *Adv. Mater.* **2016**, *28*, 6976.
[7] J. W. Sun, J.-H. Lee, C.-K. Moon, K.-H. Kim, H. Shin, J.-J. Kim, *Adv. Mater.* **2014**, *26*, 5684.
[8] C.-K. Moon, K. Suzuki, K. Shizu, C. Adachi, H. Kaji, J.-J. Kim, *Adv. Mater.* **2017**, *29*, 1606448.
[9] K.-H. Kim, J.-J. Kim, *Adv. Mater.* **2018**, *30*, 1705600.
[10] S. Y. Byeon, D. R. Lee, K. S. Yook, J. Y. Lee, *Adv. Mater.* **2019**, *31*, 1803714.
[11] T. Furukawa, H. Nakanotani, M. Inoue, C. Adachi, *Sci. Rep.* **2015**, *5*, 8429.
[12] D. Li, Y. Hu, L.-S. Liao, *J. Mater. Chem. C* **2019**, *7*, 977.
[13] K.-H. Kim, C.-K. Moon, J. W. Sun, B. Sim, J.-J. Kim, *Adv. Opt. Mater.* **2015**, *3*, 895.
[14] C. Mayr, T. D. Schmidt, W. Brütting, *Appl. Phys. Lett.* **2014**, *105*, 183304.
[15] S. Gottardi, M. Barbry, R. Coehoorn, H. van Eersel, *Appl. Phys. Lett.* **2019**, *114*, 073301.
[16] B. Perucco, N. A. Reinke, D. Rezzonico, M. Moos, B. Ruhstaller, *Opt. Express* **2010**, *18*, A246.
[17] M. Regnat, K. P. Pernstich, S. Züfle, B. Ruhstaller, *ACS Appl. Mater. Interfaces* **2018**, *10*, 31552.
[18] M. Flämmich, D. Michaelis, N. Danz, in *Proc. SPIE Int. Soc. Opt. Eng.* **2011**, *7954*, 795410.
[19] B. Perucco, N. A. Reinke, D. Rezzonico, E. Knapp, S. Harkema, B. Ruhstaller, *Org. Electron.* **2012**, *13*, 1827.
[20] Fluxim, Setfos 5.0, https://www.fluxim.com/setfos-intro/ (accessed: May 2019).
[21] B. Ruhstaller, S. A. Carter, S. Barth, H. Riel, W. Riess, J. C. Scott, *J. Appl. Phys.* **2001**, *89*, 4575.
[22] B. Ruhstaller, T. Beierlein, H. Riel, S. Karg, J. C. Scott, W. Riess, *IEEE J. Sel. Top. Quantum Electron.* **2003**, *9*, 723.
[23] B. Ruhstaller, E. Knapp, B. Perucco, N. Reinke, D. Rezzonico, F. Müller, in *Optoelectronic Devices and Properties* (Ed: O. Sergiyenko) **2011**, 978-953-307-204-3 DOI 10577214626.
[24] S.-F. Wu, S.-H. Li, Y.-K. Wang, C.-C. Huang, Q. Sun, J.-J. Liang, L.-S. Liao, M.-K. Fung, *Adv. Funct. Mater.* **2017**, *27*, 1701314.
[25] K.-H. Kim, S.-J. Yoo, J.-J. Kim, *Chem. Mater.* **2016**, *28*, 1936.
[26] Y.-S. Park, S. Lee, K.-H. Kim, S.-Y. Kim, J.-H. Lee, J.-J. Kim, *Adv. Funct. Mater.* **2013**, *23*, 4914.

[27] P. M. Borsenberger, L. Pautmeier, R. Richert, H. Bässler, *J. Chem. Phys.* **1991**, *94*, 8276.
[28] S. Noh, C. K. Suman, Y. Hong, C. Lee, *J. Appl. Phys.* **2009**, *105*, 033709.
[29] D. Yokoyama, H. Sasabe, Y. Furukawa, C. Adachi, J. Kido, *Adv. Funct. Mater.* **2011**, *21*, 1375.
[30] B. Zhao, T. Zhang, B. Chu, W. Li, Z. Su, H. Wu, X. Yan, F. Jin, Y. Gao, C. Liu, *Sci. Rep.* **2015**, *5*, 10697.
[31] M. Regnat, K. P. Pernstich, B. Ruhstaller, *Org. Electron.* **2019**, *70*, 219.
[32] V. Jankus, P. Data, D. Graves, C. McGuinness, J. Santos, M. R. Bryce, F. B. Dias, A. P. Monkman, *Adv. Funct. Mater.* **2014**, *24*, 6178.
[33] M. Pope, C. E. Swenberg, *Electronic Processes in Organic Crystals and Polymers*, Oxford University Press, Oxford **1999**.
[34] H. van Eersel, P. A. Bobbert, R. A. J. Janssen, R. Coehoorn, *J. Appl. Phys.* **2016**, *119*, 163102.
[35] D. Berner, F. Nuesch, E. Tutiš, C. Ma, X. Wang, B. Zhang, L. Zuppiroli, *J. Appl. Phys.* **2004**, *95*, 3749.
[36] B. Sim, C.-K. Moon, K.-H. Kim, J.-J. Kim, *ACS Appl. Mater. Interfaces* **2016**, *8*, 33010.
[37] S. Reineke, F. Lindner, Q. Huang, G. Schwartz, K. Walzer, K. Leo, *Phys. Status Solidi B* **2008**, *245*, 804.
[38] Paios, Platform for All-In-One Characterization of Solar Cells and OLEDs, Characterization Suite Software version 4.12, Fluxim, https://www.fluxim.com/paios/ (accessed: May 2019).